

**Dynamics of washboard road formation driven by a harmonic oscillator**Teeranai Srimahachota,<sup>1</sup> Hao Zheng,<sup>2</sup> Motohiro Sato,<sup>2</sup> Shunji Kanie,<sup>2</sup> and Hiroyuki Shima<sup>3,\*</sup><sup>1</sup>*Graduate School of Engineering, Hokkaido University, Kita 13 Nishi 8, Kita-ku, Sapporo 060-8628, Japan*<sup>2</sup>*Faculty of Engineering, Hokkaido University, Kita 13 Nishi 8, Kita-ku, Sapporo 060-8628, Japan*<sup>3</sup>*Department of Environmental Sciences, University of Yamanashi, 4-4-37, Takeda, Kofu, Yamanashi 400-8510, Japan*

(Received 21 August 2017; revised manuscript received 14 November 2017; published 13 December 2017)

Granular surfaces subjected to repeated passage often spontaneously develop a corrugated pattern. In this study, we scrutinized the growth dynamics of surface corrugation in a self-rotating sand bed that is traced by the edge of a vertically oscillating arm. We found that both the rotation velocity and the frequency of the oscillator strongly affect the occurrence rate of corrugation as well as the time evolution in the corrugation pattern, due to the intermittent collision between the oscillator and sand bed. We also discovered that the growth dynamics involves two distinct collective modes that describe the translational motion of the corrugation pattern on the sand bed.

DOI: [10.1103/PhysRevE.96.062904](https://doi.org/10.1103/PhysRevE.96.062904)**I. INTRODUCTION**

Washboarding is the spontaneous formation of a transverse ripple on a dirt road. It is usually found on unpaved, heavy-traffic roads under dry weather conditions, causing discomfort to drivers and occupants in vehicles traveling on the road due to the unpleasant vibration. The transverse ripple may also increase the risk of traffic accidents because it reduces the contact area of the wheel to the road surface and thus degrades the operability of the vehicle. Mitigation of the washboarding, therefore, has long been a challenge for road maintenance [1,2]. In addition to the practical importance, washboarding has drawn much attention from academic scientists. This is primarily because the spontaneous formation of a periodically corrugated pattern, similar to washboarding, is commonly observed in a variety of physical systems with different material components; examples include railway tracks [3–5], sand beds underneath flowing fluid [6–8], lubricated disks [9,10], and periodic ripple on snow-covered roads [11].

The mechanism of washboarding on dirt roads was first considered in 1962 by Mather [12], who concluded that it originates from the bouncing motion of the wheel when it is excited by random irregularity of the road surface. Afterwards, a series of experimental works proved that the wheel bouncing is not a necessary condition; a rolling wheel [13] and an incline plow dragged on a granular roadbed [14–18] can trigger the surface corrugation even when they stay in contact with the roadbed. The experimental findings on granular roadbed corrugation under the keep-in-touch condition can be described in part by theoretical models [19,20], which uncovered that the lift and drag forces acting on the dragged object, as well as the pulling velocity, play the role of deterministic parameters in the time variation of the surface geometry [15,18,21].

In the present work, we revisited the earlier-reported mechanism of surface corrugation, i.e., the granular roadbed corrugation excited by the periodic bouncing of a dragged object [12,22–24]. We hypothesized that the bouncing effect on temporal growth of corrugation should be altered qualitatively

by attaching a vertically oscillating device (i.e., a mechanical spring) to the dragged object. For instance, the restoring force exerted by the spring will facilitate an upward jump of the horizontally dragged object, which is triggered by collision with a bump on the roadbed. Furthermore, the vertical oscillation of the object will result in a quasiperiodic collision with the roadbed surface, giving rise to corrugation with a wavelength that depends on the horizontally pulling velocity of the object and the natural frequency of the spring. These imply the interdependence of the time evolution in the corrugation pattern with mechanical parameters of the system, while quantitative examination has lagged so far.

To verify the hypothesis mentioned above, we conducted the washboard road experiment using a self-rotating granular roadbed. The surface of the roadbed was traced by an edge of a balanced lever (i.e., oscillator), which can swing vertically around a pivot while attached to a spring that drives quasiperiodic oscillation. By iteratively changing the rotation velocity and the frequency of the oscillator, we examined the requisite conditions for surface corrugation to occur. We also scrutinized the role of the two mechanical parameters in the subsequent growth of surface corrugation. Eventually, the corrugation patterns showed nonmonotonic time variation with respect to both the amplitude and wavelength, depending on the two parameter settings.

**II. EXPERIMENTAL SETUP****A. Self-rotating track**

Figure 1 illustrates the developed experimental apparatus. It consists of a self-rotating roadbed track, seesaw-shaped oscillator, and laser range finder. The latter two devices are fixed at a cantilever beam that extends from the rotational axis of the track, as depicted in Fig. 1(b). The roadbed track rotates with respect to the fixed devices by a rotation velocity, designated by  $v$ . The velocity can be continuously tuned from 0 up to 20.0 rounds per minute (rpm); the maximum value of  $v$  corresponds to ca. 0.5 m/s in the relative speed of the track with the fixed devices.

The outer and inner circular boundaries of the track are 59 and 41 cm in diameter, respectively. The gap between the

\*hshima@yamanashi.ac.jp

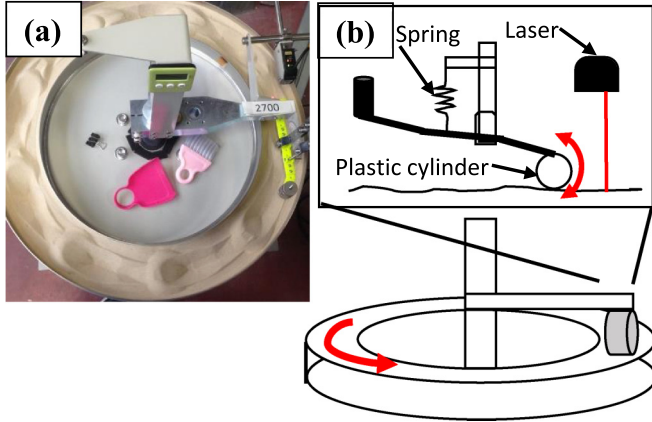


FIG. 1. Schematic illustration of the experimental apparatus. (a) Snapshot of the corrugation experiment. The top surface of dried sand bed in an annulus container shows several ripples that form periodically in the circumferential direction. (b) Diagram of the seesaw-shaped oscillator that consists of a plastic cylinder, counterweight, and a soft spring. A laser range finder is also sketched.

two circular boundaries is filled with dry granular sand, called Toyoura sand, with particle size of  $0.2 \pm 0.1$  mm. Toyoura sand is well-studied Japanese silica sand [25], and has been widely used as a standard material for physical model tests.

The time variation in the sand surface height during experiments was probed at 100-Hz intervals using the laser range finder with  $1 \mu\text{m}$  precision [see Fig. 1(b)]. The data obtained were used to analyze the geometric feature of the corrugated pattern at a certain moment and the time evolution of the pattern throughout an experiment.

### B. Seesaw-shaped oscillator

The seesawlike oscillator, depicted in Fig. 1(b), plays a key role in our corrugation experiments. The total length of the oscillator is 14.2 cm, and one end is attached to a circular piece of cylinder, made from ABS plastic (acrylonitrile butadiene styrene), 3 cm in diameter, 1.5 cm width, and 5.2 g in weight. This plastic cylinder cannot roll but is dragged simply on the roadbed surface. The other end of the seesaw is loaded by a few coins as a counterweight; the coins are fixed firmly to the end by nuts and bolts. The middle part of the seesaw was suspended by a mechanically soft spring (spring constant of 85.3 N/m), which promotes the vertical oscillation of the cylinder. The oscillation frequency can be regulated by changing the number of coins as the counterweight, as explained later (see Sec. II C).

Before the roadbed rotation starts, we set the oscillator to be in balance of force while the bottom edge of the cylinder gently touched the flat sand surface with almost no compressive force against the surface. This balance in forces should be kept even after the roadbed rotation starts, provided the sand surface would be ideally flat. In reality, however, collision of the cylinder with an infinitesimal bump that is inevitably present on the almost-flat surface breaks the balance of force, and it triggers an upward jump of the cylinder followed by a knock on the sand surface from above. As a result of the hammerlike knock, a small pit and a pair of small bumps form locally, and they then trigger another jump-and-knock

event that will generate another, larger undulation on the sand surface. Through this repetitive process, periodic surface corrugation may form if conditions permit.

### C. Natural frequency of oscillator

The natural frequency of the seesaw-shaped oscillator,  $f$ , was controlled by changing the counterweight at the tail of the oscillator. To determine the value of  $f$ , we first cleared out the sand container in the track and freely oscillated the seesaw with a small amplitude. Next, the vertical displacement of the cylinder was monitored using a laser range finder. The time series data were then converted to the frequency spectrum using the fast Fourier transform (FFT) technique. Finally, the primary peak position in the spectrum allowed us to define  $f$ .

In the actual experiments, we set the counterweight so that  $f$  was equal to 1.36, 1.46, or 1.66 Hz; the corresponding counterweights were 110, 99.0, and 79.2 g, respectively. For any of the values of  $f$  and for any value of  $v$  within the range listed in Sec. II A, the seesaw shows several (typically four to 12) vertical swings in one round of the rotating track.

### D. Sand-bed preparation

Before launching the experiment, we uniformly leveled the sand layer to a thickness of 3.0 cm over the entire track with an accuracy of  $\pm 2$  mm. Next, we rotated the track at 3.0 rpm (0.08 m/s) for 2 min to stabilize the sand layer. At this stage, the oscillator did not contact the surface of the sand. During the rotation, we recorded the height of the sand surface using the laser and used the result afterwards to derive the average height of the original surface over the track.

Once the preparation was completed, we placed the edge of the oscillator gently on the surface while keeping the 3.0 rpm track rotation. We then quickly raised the rotation velocity to a desired value (within the range of 6.0 to 19.5 rpm) and recorded the time variation in the height of the sand surface for 7 min. Such 7-min duration experiment was repeated three times for every choice of the paired parameter settings:  $v$  and  $f$ . In order to prevent a compaction effect, the whole sand layer was loosened every after several 7-min duration experiments.

The criteria for determining the presence or absence of the corrugation development was as follows: (i) If the surface stays flat or runs smooth after a 7-min experiment, we say “no corrugation form”; (ii) if there is no single predominant peak in the FFT spectrum of the sand surface [see Fig. 5(a)] even after a 7-min trial, we say “no corrugation form” in the trial. However, we never encountered the case of (ii) throughout the present work, whenever a certain degree of corrugation was visibly recognized.

## III. SPATIAL PROFILE OF CORRUGATION

### A. Maximum height of corrugation

The height of sand piles that form in a well-grown corrugation is a visible measure that quantifies the geometric profile of the corrugated surface. It is defined by the distance from the average height of the original flat surface to the top of a pile. An interesting observation in our experiment was that the maximum height of piles among those found during one

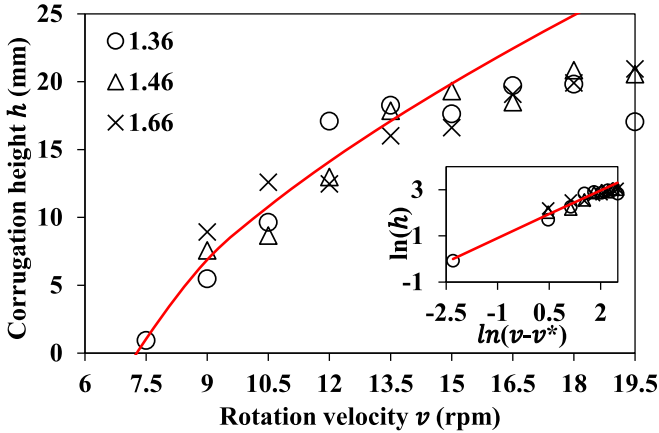


FIG. 2. Maximum height of corrugation that develops during the 7-min track rotation. Every data point indicates the mean value of the maximum sand pile heights over one to three trials. A plausible fitting curve based on Eq. (1) is also plotted. Inset: Logarithm plot of the data.

trial (i.e., a 7-min track rotation) was systematically dependent on  $v$ . In broad terms, the faster the track rotates, the higher the piles grow as explained below.

Figure 2 shows the  $v$  dependence of the maximum pile height. Every data point in the plot indicates the average value of the maximum heights among a few (one, two, or three) trials during which corrugation formed (at  $v = 6.0$  rpm, no corrugation appeared for every choice of  $f$ ). Figure 2 illustrates that a fast rotation of the track promotes the growth of the pile height, as is consistent with previous studies on corrugation under the keep-in-touch condition [13–15]. It was also found that the variation in  $f$  gives little effect on the  $v$  dependence of the maximum height of the sand piles, denoted by  $h(v)$  hereafter, at least within the range of  $f$  we have explored.

The inset in Fig. 2 gives a logarithm plot of the same data as in Fig. 2. The data points at  $v \leq 13.5$  rpm seem to collapse onto a plausible fitting curve expressed by

$$h(v) = h^*(v - v^*)^\alpha, \quad (1)$$

with  $h^* = 5.0$  mm,  $v^* = 7.4$  rpm, and  $\alpha = 0.68$ . At  $v$  larger than 13.5 rpm, the data points deviate feasibly downward from the fitting curve, possibly because of the landslide along the slope of the sand pile. The power-law form shown in Eq. (1) is commonly observed in the pitchfork bifurcation phenomenon [26,27], which is a specific class of local bifurcation where the system transitions from one fixed point to three fixed points (two stable and one unstable). The precise functional form of the fitting curve as well as its physical interpretation are yet to be debated; nevertheless, it would be fair to conclude from Fig. 2 that  $h(v)$  increases monotonically with  $v$  above a threshold  $v^*$  that serves as the critical velocity for the occurrence of corrugation.

It is also important that although corrugation does not always form at a given choice of  $v$  and  $f$ , when it does, the threshold value of  $v^*$  and the power-law fitting curve shown in Fig. 2 are reproducible. Particularly near the threshold, any instability in the surface geometry is very sensitive to small

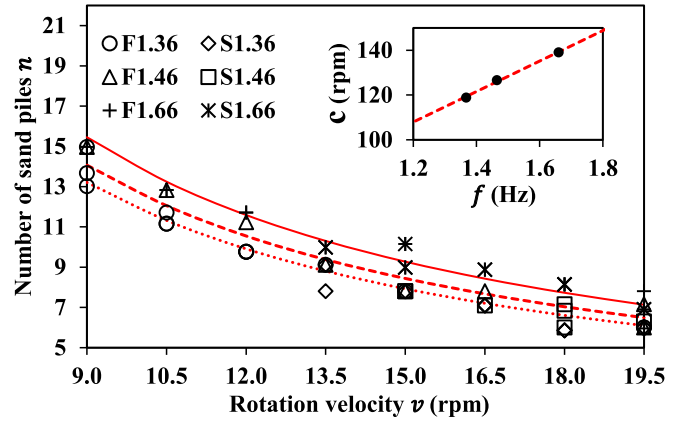


FIG. 3. Number of sand piles obtained after the completion of the 7-min track rotation. In the legend, “F” represents the forward-moving mode, and “S” represents the stationary mode; see text in Sec. VB for the definitions of the two modes. Inset: The proportional constant  $c$  given in Eq. (2) as a function of  $f$ .

irregularities; therefore, the number of 7-min trials during which corrugation formed showed strong fluctuation. This is the reason why no data point appears both for  $f = 1.46$  Hz and 1.66 Hz at  $v = 7.5$  rpm as shown in Fig. 2.

### B. Total number of sand piles

Figure 3 shows the number of sand piles,  $n$ , that formed in the corrugated surface after the 7-min track rotation. To evaluate  $n$  in experiments, we picked up the time-series data of the sand surface height only within the final round of the track rotation. Then we converted the data to an FFT spectrum in order to find the position of the highest primary peak, which allowed us to identify the characteristic wavelength,  $\lambda$ , that is the most dominant component in the corrugation profile. By dividing the one-round perimeter of the track,  $L$  ( $\approx 157$  cm), by  $\lambda$ , we estimated  $n$ , which appeared at the final stage. The symbols “F” and “S” in the legend of Fig. 3 indicate the direction of the collective translational motion of the corrugation pattern during the 7-min rotation, as explained later (see Sec. VB).

Figure 3 shows that  $n$  decreases gradually with  $v$ . This decreasing trend, commonly observed for different values of  $f$ , is intuitively understood; the faster rotation of the track causes both the larger oscillation amplitude of the cylinder and the longer distance between adjacent landing positions, thus leading to the longer wavelength of the periodic corrugation profile and the smaller number of ripples contained within a finite perimeter length of the track.

Particular attention should be paid to the data seeming to obey an inversely proportional relation described by

$$n = c/v. \quad (2)$$

The corresponding fitting curves for each data set obtained under a specific  $f$  value among the three choices are depicted in Fig. 3. The proportionality constant,  $c$ , increases almost linearly with  $f$ , as summarized in the inset of Fig. 3. This  $f$  dependence of  $c$  is explained by the following two reasons. One reason is that the higher-frequency oscillation of the

cylinder gives rise to a higher number of sand piles on the sand surface at a fixed  $v$ , thus causing an increase in  $c$ . The other reason is based on the change in the inertia of the swinging arm. We have mentioned in Sec. II C that  $f$  is controlled by the counterweight at the tail of the arm. For a greater mass, therefore, the mechanical impact of the cylinder against the sand bed becomes greater, causing penetration under the sand surface. This penetration yields an enhanced drag force, thus hindering the upward jump of the cylinder. As a consequence, the cylinder's oscillation with a greater mass (i.e., with a lower  $f$ ) provides a smaller value of  $c$  as shown in the inset of Fig. 3.

If we introduce an effective frequency of the oscillator,  $f^*$ , defined by

$$f^* = v/\lambda, \quad (3)$$

then we have

$$f^* = c/(n\lambda) = c/L. \quad (4)$$

Thus, from the inset of Fig. 3,  $f^* = 0.757$  Hz for  $f = 1.36$  Hz,  $f^* = 0.806$  Hz for  $f = 1.46$  Hz, and  $f^* = 0.886$  Hz for  $f = 1.66$  Hz. These results mean that the frequency of the oscillator that we observed during the experiment should be ca. 55% of the original natural frequency due to the drag force exerted by the rotating sand bed. More precisely, the ratio  $f^*/f$  is slightly decreasing with  $f$ : It reads 0.557 for  $f = 1.36$  Hz, 0.552 for  $f = 1.46$  Hz, and 0.534 for  $f = 1.66$  Hz. This decreasing behavior of  $f^*/f$  is also attributed to the inertia-induced enhancement in the drag force, as discussed above.

#### IV. LATERAL DYNAMICS OF CORRUGATION

##### A. Sand pile reconstruction at transient state

Once a sand pile forms on the initially flat surface, the vertical height and lateral position can shift intermittently due to repeated collisions with the oscillating cylinder. This holds true even for the piles consisting of a well-grown corrugated sand surface. Therefore, both the amplitude and wavelength of the surface corrugation can alter with time either swiftly or gradually depending on the situation as explained below.

Figure 4 shows the space-time diagrams that illustrate the dynamics of corrugation outlined above. The plots demonstrate the time variation in the height of the surface beneath the laser range finder. The vertical axis,  $R$ , indicates the number of rotations of the track with respect to the fixed laser. The horizontal axis indicates the elapsed time during each round of the track rotation. Therefore, the horizontal array of data points that line up at  $R = N$  ( $N = 1, 2, 3 \dots$ ) gives the sand surface profile along the circumferential direction just at the completion of  $N$ -rounds rotation.

As suggested in Fig. 4, only a few track rotations suffice to obtain visible undulation in the initially flat sand surface and a precursor of corrugated pattern. As time passes, the early-stage corrugated pattern often falls into a so-called *transient state*. In the transient state, the motion of the oscillator becomes irregular and adjacent piles merge to break each other. Due to this destructive process, the height of piles stops increasing and

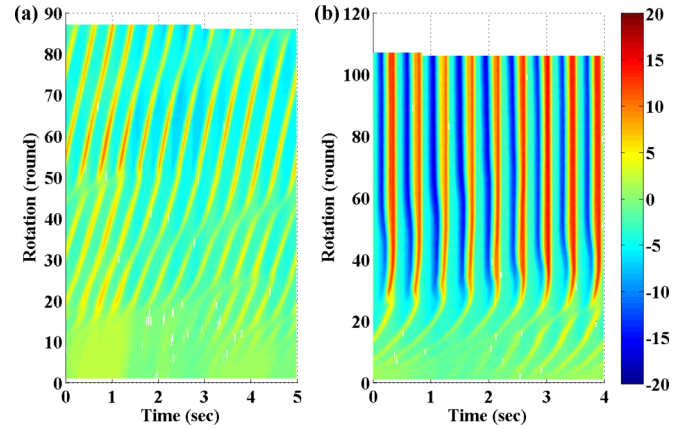


FIG. 4. Space-time diagrams showing the time development of corrugation at  $v = 12.0$  rpm (a) and  $v = 15.0$  rpm (b). The color strip represents the height of the sand surface at a point just below the fixed laser in units of millimeters.

even decreases. It lasts typically about—ten to 15 rotations, during which one ripple disappears. After a transient state, another corrugated pattern with reduced  $n$  (and thus reduced  $\lambda$ ) emerges and the motion of the oscillator becomes stable again.

A transient state does not necessarily happen only once. In fact, we have sometimes observed transient states several times in one 7-min trial. Overall, the faster the track rotates, the more often the transient state occurs in the first half of the 7-min trial. It was also found that a transient state tends to take place just after a certain corrugated pattern is well developed.

One potential reason behind the occurrence of transient states is the out-of-phase oscillation of the cylinder with respect to the existing periodic array of sand piles on the surface. The number of piles on the track with a finite-length perimeter must be an integer. In contrast, the number of the cylinder swings per round may not always be an integer. Because of the mismatch between them, phase lag in the oscillation accumulates with time, eventually causing the emergence of a transient state that destructs a certain pile.

##### B. Forward-moving mode vs stationary mode

Another important observation illustrated in Fig. 4(a) is the translational motion of the whole corrugation pattern over time. For instance, the diagram is covered by many slanted, striped lines that are parallel; the slope angle of the stripe lines indicates the migration speed of the periodically aligned sand piles in the circumferential direction.

Note that the striped lines are slanted diagonally up and right. This represents that all the ripples moved forward throughout a 7-min rotation of the track.

Similar collective movement of the corrugation in the forward direction was observed in Fig. 4(b), too, although it persists during only the first 30 rotations. After the first 30 rotations, the forward-moving mode terminates at a transient state, and then the corrugated pattern becomes stationary with respect to the rotating reference frame. The latter state of the unmoving corrugation, called the stationary mode, is

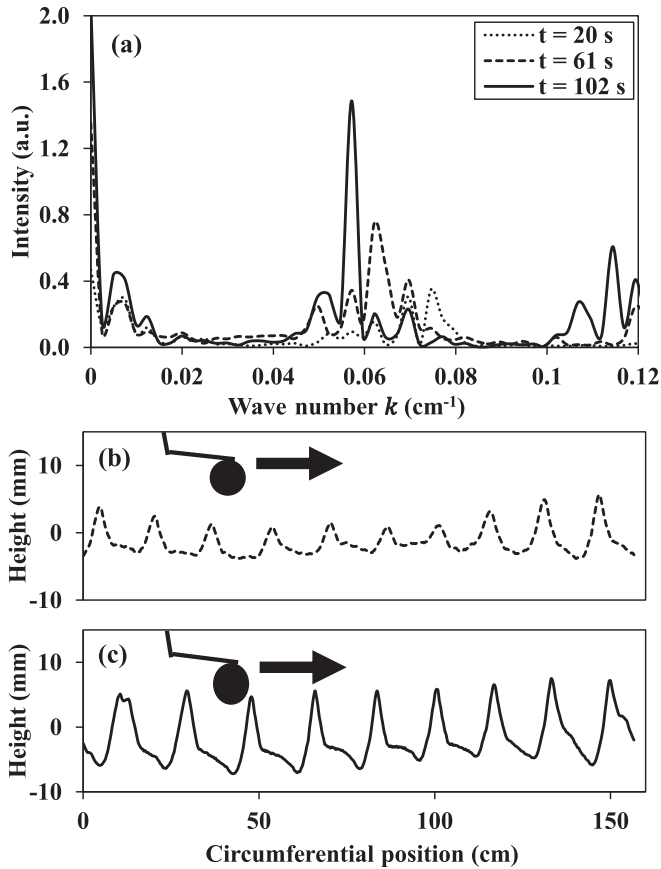


FIG. 5. (a) FFT spectrum of the sand surface corrugation obtained at three different elapsed times. (b) The real-space profile of the surface corrugation at  $t = 61$  s. (c) The profile at  $t = 102$  s. The parameters  $v$  and  $f$  are set at the same values as in Fig. 4(b).

manifested in the vertically aligned striped lines shown in the upper two-thirds of the space-time diagram in Fig. 4(b).

### C. Stepwise shift in the FFT peak position

Figure 5 illustrates the effects of mode switching on the FFT spectrum of the surface corrugation [Fig. 5(a)] and the corrugation profile in real space [Figs. 5(b) and 5(c)]. The parameters  $v$  and  $f$  are set equal to those in Fig. 4(b). We observe that the FFT spectrum undergoes a stepwise shift in the peak position and a gradual change in the peak intensity. At the first stage of a 7-min trial, several peaks with low intensity appeared around the wave number  $k \approx 7 \times 10^{-2} \text{ cm}^{-1}$ . As time passes, one of those peaks begins to be enhanced in amplitude, resulting in the spectrum shown by a dashed curve in Fig. 5(a);  $t = 61$  s. This growth of a specific peak at  $k \approx 6.2 \times 10^{-2} \text{ cm}^{-1}$  originates from a growth of a corrugation with the characteristic wavelength  $\lambda = 2\pi/k \approx 16$  cm. Afterwards, the system reaches a transient state followed by swift enhancement of an alternative peak positioned at lower  $k (\approx 5.8 \times 10^{-2} \text{ cm}^{-1})$ , as shown in Fig. 5(a) by a solid curve;  $t = 102$  s. The last enhanced peak survives until the end of a 7-min trial, thus indicating the sand surface profile in a well-grown corrugation at the final stage. It should be noted that, during the successive shift in the peak position, only a

few values of  $k$  are allowed as the peak position since they must be equal to the track's perimeter divided by an integer.

Figures 5(b) and 5(c) exhibit the surface profiles that correspond to the FFT spectra at  $t = 61$  s and  $t = 102$  s, respectively. The spatial uniformity in the corrugation amplitude is clearly observed in Fig. 5(c), which is consistent with the high intensity of the enhanced peak in the FFT spectrum. The number of sand piles detected in Fig. 5(c) is a bit smaller than in Fig. 5(b), indicating the disappearance of several sand piles during the transient state.

A noteworthy finding in the final-stage FFT spectrum shown in Fig. 5(a) is the emergence of an overtone peak at  $k \approx 0.114 \text{ cm}^{-1}$ . This overtone peak is a result of geometric asymmetry in individual sand piles that constitute the well-grown corrugation. Figure 5(c) shows that the slope gradient of the sand piles is high at the front face with respect to the collision with the cylinder. At the back face, on the other hand, shoulderlike small bumps of various heights are formed. This asymmetry in the sand pile shape is reminiscent of a “hoeinglike” collision between the cylinder and the front face of the sand piles, thus yielding a spectral component of the twofold overtone periodicity ( $\approx \lambda/2$ ) that is superposed to the original periodicity ( $\approx \lambda$ ) in the corrugated surface. Eventually, the overtone peak emerges in the FFT spectrum as the signature of the completion of corrugation growth.

### D. $v$ -Dependent likelihood of the mode occurrence

Our extensive measurement with iterative changes in  $v$  and  $f$  revealed the tendency in the occurrence of the two collective modes as follows: (i) the forward-moving mode is likely to persist throughout the whole 7-min duration if we set low  $v$  (e.g., 12.0 rpm and slower), and (ii) the mode switching from the forward-moving to the stationary mode at a few tens of rotations is likely to happen at high  $v$  (e.g., 13.5 rpm and faster). These findings are summarized in Fig. 3, in which different symbols are used to categorize the two different collective modes observed at the final stage of a 7-min trial. Corrugation always moves forward at the beginning of a trial. It was also confirmed that the tendencies mentioned above are independent of the change in  $f$ , at least within the frequency range we have examined. This result is in part consistent with the previous studies using a rolling wheel [13] and plow [14]. Nevertheless, in this study, both forward and stationary ripples were observed in the same trial.

The likelihood of the forward-moving mode at small  $v$  and the stationary mode at large  $v$  is attributed to the  $v$ -dependent bouncing motion of the cylinder as discussed below. Figure 6 is a diagram of the way the cylinder leaps a sand pile after collision with the sand bed located in front of the pile. When  $v$  is small [see Fig. 6(a)], the collision-driven impulsive force applied to the cylinder is weak and thus the vertical jump height of the cylinder is not enough to leap the sand pile. As a result, the cylinder collides with both the front surface and the upper part of the sand pile, then pushes a large amount of the sand particles forward. This hoeinglike behavior of the cylinder is likely to happen either when  $v$  is small, or when the vertical amplitude of the oscillation has not yet sufficiently grown, or both. The latter undeveloped-oscillation-induced hoeing of the

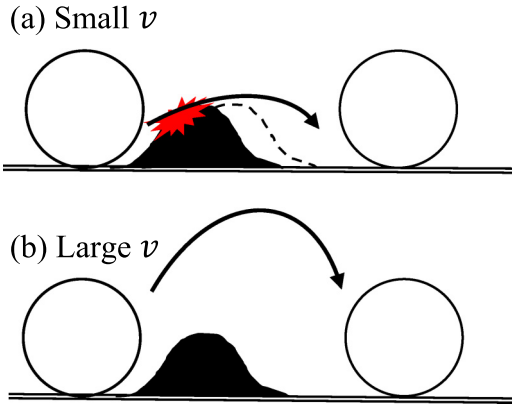


FIG. 6. Jumping motion of the cylinder in the vicinity of a sand pile. Collision with the upper portion of a pile at small  $v$  and overleap at large  $v$  are depicted in the panels (a) and (b), respectively.

cylinder is the reason why the forward-moving mode is always observed at the beginning of the experiment.

A parallel argument to the one above explains the occurrence of the stationary mode at large  $v$  in high probability. When  $v$  is large enough [see Fig. 6(b)], the impulsive force applied to the cylinder at the early stage of a 7-min rotation is so strong that the accumulation of that force will yield a large-amplitude oscillation of the cylinder in a relatively short time, compared to the small- $v$  case. Therefore, if the characteristic wavelength of the cylinder's oscillation on the sand bed is a multiple of the wavelength in well-grown corrugation, the cylinder jumps over every sand pile without any collisions with the upper portion of the pile. Eventually the system falls into the stationary mode in which none of the piles move with respect to the rotating frame.

## V. SUMMARY

We investigated the spontaneous corrugation of a self-rotating sand surface traced by an oscillator. The main findings obtained are listed below.

- (i) A threshold rotation velocity  $v^*$  above which corrugation occurred was found to exist. The value of  $v^*$  was insensitive to the change in the oscillation frequency  $f$ .
- (ii) The height of surface corrugation,  $h(v)$ , turned out to be an increasing function of  $v$  with obeying a power-law form of  $h(v) \sim (v-v^*)^\alpha$ .
- (iii) The setting of  $v$  strongly affected the geometric attributes of the final corrugation pattern (e.g., wavelength and amplitude); the faster the sand bed rotated, the larger the corrugation amplitude was reached with longer wavelength.
- (iv) During the growth of corrugation, there were two distinct collective modes in the translational motion of corrugation: the forward-moving mode and the stationary mode. The former mode took place whenever the corrugation started to grow; undergoing one or more transient states, the system sometimes reached the stationary mode. The mode switched as a consequence of the oscillator-driven reconstruction of the sand pile arrangement on the sand bed.

## ACKNOWLEDGMENTS

The authors would like to thank Ms. Aiko Ikeda for technical assistance. This work was supported by KAKENHI Grants No. 25390147, No. 16K01278, and No. 16K12823.

- 
- [1] H. Mahgoub, C. Bennett, and A. Selim, *Transp. Res. Rec.* **2204**, 3 (2011).
  - [2] A. Alhasan, D. J. White, and K. De Brabanter, *Transp. Res. Rec.* **2523**, 105 (2015).
  - [3] Y. Sato, A. Matsumoto, and K. Knothe, *Wear* **253**, 130 (2002).
  - [4] S. L. Grassie and J. W. Edwards, *Wear* **265**, 1150 (2008).
  - [5] K. H. Oostermeijer, *Wear* **265**, 1231 (2008).
  - [6] F. Engelund and J. Fredsoe, *Annu. Rev. Fluid Mech.* **14**, 13 (1982).
  - [7] O. Terzidis, P. Claudin, and J.-P. Bouchaud, *Eur. Phys. J. B* **5**, 245 (1998).
  - [8] F. Zoueshtiagh and P. J. Thomas, *Phys. Rev. E* **67**, 031301 (2003).
  - [9] Q. Dai, F. Hendricks, and B. Marchon, *J. Appl. Phys.* **96**, 696 (2004).
  - [10] Q. Dai, F. Hendricks, and B. Marchon, *IEEE Trans. Magn.* **40**, 3159 (2004).
  - [11] S. Kanie, Z. Hao, D. Yokomise, Y. Kaneda, Y. Nagata, and S. Masaki, *Annu. Rep. Snow Ice Stud. Hokkaido* (in Japanese) **35**, 55 (2016).
  - [12] K. B. Mather, *Sci. Am.* **208**, 128 (1962).
  - [13] N. Taberlet, S. W. Morris, and J. N. McElwaine, *Phys. Rev. Lett.* **99**, 068003 (2007).
  - [14] A.-F. Bitbol, N. Taberlet, S. W. Morris, and J. N. McElwaine, *Phys. Rev. E* **79**, 061308 (2009).
  - [15] B. Percier, S. Manneville, J. N. McElwaine, S. W. Morris, and N. Taberlet, *Phys. Rev. E* **84**, 051302 (2011).
  - [16] I. J. Hewitt, N. Balmforth, and J. N. McElwaine, *J. Fluid Mech.* **692**, 446 (2012).
  - [17] I. J. Hewitt and N. Balmforth, *J. Non-Newtonian Fluid Mech.* **169-170**, 74 (2012).
  - [18] B. Percier, S. Manneville and N. Taberlet, *Phys. Rev. E* **87**, 012203 (2013).
  - [19] S. Shoop, R. Haehnel, V. Janoo, D. Harjes, and R. Liston, *J. Geotech. Geoenviron. Eng.* **132**, 852 (2006).
  - [20] Y. Zhang, P. Xiao, T. Palmer, and A. Farahani, *SAE Technical Paper 980900* (1998).
  - [21] N. Gravish, P. B. Umbanhowar, and D. I. Goldman, *Phys. Rev. Lett.* **105**, 128301 (2010).
  - [22] J. A. Both, D. C. Hong, and D. A. Kurtze, *Physica A* **301**, 545 (2001).

- [23] N. P. Hoffmann and U. Stolz, *Wear* **268**, 886 (2010).
- [24] D. A. Kurtze, D. C. Hong, and J. A. Both, *Int. J. Mod. Phys. B* **15**, 3344 (2001).
- [25] K. Nakarai and T. Yoshida, *Soil Found.* **55**, 857 (2015).
- [26] A. Juel, A. G. Darbyshire, and T. Mullin, *Proc. R. Soc. London, Ser. A* **453**, 2627 (1997).
- [27] S. H. Strogatz, *Nonlinear Dynamics and Chaos: With Applications to Physics, Biology, Chemistry and Engineering*, 2nd ed. (Westview Press, Boulder, CO, 2014).